Mass-Dimensional Relationships for Ice Particles and the Influence of Riming on Snowfall Rates

DAVID L. MITCHELL, RENYI ZHANG AND RICHARD L. PITTER

Desert Research Institute, University of Nevada, Reno, Nevada

(Manuscript received 14 April 1989, in final form 8 September 1989)

ABSTRACT

The masses, dimensions, and habits of over 2800 natural ice particles precipitating from orographic winter storms in the central Sierra Nevada were obtained using photomicrographs. Ice particles that could be unambiguously classified were used to generate empirical expressions relating snow particle masses and dimensions. Many of the ice particle types had not been investigated previously. The influence of riming and aggregation on ice particle masses was examined. When possible, comparisons are made between these results and those of other experimental observations. By incorporating these mass-dimensional relationships into an expression for the ice mass content in a snowstorm, it was possible to estimate the mass fraction of the fresh snowpack resulting from accreted supercooled cloud water. The results from two storms analyzed suggest that about 30 to 40 percent of the deposited snow is composed of accreted cloud water during moderately rimed snowfall.

1. Introduction

An understanding of the development of precipitation in glaciated or mixed-phase clouds often requires knowledge of the size dependence of ice particle masses. For instance, power law mass-dimensional relationships are useful in field studies investigating precipitation development and cloud dynamics in snowing clouds (Herzegh and Hobbs 1981). The vertical evolution of the ice mass content and snowfall rate within clouds may be evaluated by combining appropriate fallspeed- and mass-dimensional relationships with laser imaging probe measurements of snow-size spectra.

Power law mass-dimensional expressions (Locatelli and Hobbs 1974) have also been used in microphysical models (Mitchell 1988) to help determine the rates of ice particle growth by vapor diffusion and aggregation. As advances are made in modeling precipitation processes, the need for more detailed information regarding ice particle mass-dimensional relationships should become more acute.

A number of studies have been conducted on the masses of natural ice particles (e.g., Nakaya and Terada 1935; Bashkirova and Pershina 1964; Zikmunda and Vali 1972; Locatelli and Hobbs 1974). The mass measurements of Locatelli and Hobbs (1974) in the Cascade Mountains are probably the most extensive to date, giving information on the mass variation with respect to size for aggregates and rimed particles of different densities and types. However, in view of the wide variety of ice crystal habits (Magono and Lee 1966), and the varying degrees of riming and aggregation possible with different crystal habits, there are still many ice particle types for which mass-size characterizations have not been made.

This paper presents the results of observations of the masses and sizes for a variety of ice particle types obtained during the winter seasons of 1985–86 and 1986–87 in the central Sierra Nevada. The effects of riming and aggregation on ice particle mass-size relationships are examined. The mass-size expressions are then compared with those from similar studies to examine the degree of variability of a given mass-size relationship that arises from different studies using different methods at different locations. Such comparisons are necessary before these relationships can be applied with confidence.

Few field studies have estimated the contribution of accreted supercooled cloud water to the snowfall rate. Feng and Grant (1982) found that, for the same number flux, the snowfall rate for rimed plates and dendrites was about twice the snowfall rate for unrimed plates and dendrites. This implies that, for rimed snowfall, about half of the ice mass flux was derived from accreted cloud water and the other half resulted from the diffusional growth of ice. Another experimental study by Harimaya and Sato (1989) yielded a similar result, with riming generally contributing about 40 to 60% of the ice mass in rimed snowflakes. Using measurements from aircraft flying over the Sierra Nevada, Marwitz (1986) compared calculated condensation supply rates with calculated depletion rates from diffusional growth

Corresponding author address: David L. Mitchell, Atmospheric Sciences Center, Desert Research Institute, P.O. Box 60220, 5625 Fox Avenue, Reno, NV 89506-0220.

and accretion. He concluded that over half of the condensate supplied by the updraft was probably depleted via accretion. In this study, mass-dimensional expressions for rimed and unrimed ice particles of the same type are used in combination with an expression for the ice mass concentration to estimate the effect of riming on snowfall rates.

2. Procedures

The ground microphysics obserations described in this study were made in the Sierra Nevada of California, 8 km northeast of the Donner Pass, at an elevation of 2.1 km. Winds during snowstorms are usually westerlies in this region. The sampling site was on the lee side of the mountain crest, which ranges from 2.6 to over 3.0 km in elevation. Temperatures during sampling ranged from 0° to −5°C.

Snow particles were collected using a small plastic plate or petri dish. The dish was exposed in a horizontal orientation for about 3 to 60 seconds, depending on the snowfall rate. Exposure time was varied to get a representative sample, and yet to minimize the overlap of crystals on the dish. Samples were taken every 10 to 15 minutes. Tall conifers surrounded the clearing at the site, resulting in generally light winds during sampling. Care was exercised to avoid sampling when there was danger of contamination from blowing snow. The measured sizes of aggregates may be inflated somewhat over their freefall dimensions, since aggregates tend to flatten upon impact. Two photographs were taken for each sample. The first photograph showed the ice particles themselves, while the second showed the freshly melted drops. During the winter of 1985–86, close-up lenses affixed to a 35-mm camera were used to magnify the particles, while for the winter of 1986–87, a stereo microscope with a camera attachment was used. Data from this last season will be presented separately due to the different photographic techniques used, and to allow for uncertainty estimates to be made for the power law coefficients.

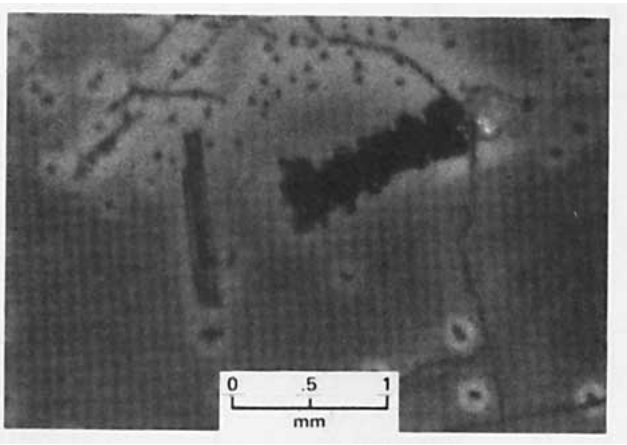

FIG. 2. Examples of rimed and unrimed long columns from the 1986–87 field season. The small specks are frost particles that formed on the petri dish.

Analysis of the photographic data was made by projecting the negative images of the black and white slides onto a screen. This resulted in magnifications of 25× when the close-up lenses were used and 106× when the microscope was used. A portion of a photomicrograph from the 1985–86 field season, showing long columns as the most abundant particle type, is shown in Fig. 1, while long columns from the 1986–87 field season are shown in Figs. 2 and 3. Figures 1 and 3 approximately reflect differences in magnification experienced during sample analysis (differences were slightly greater than this). The measurement technique during both field seasons was sensitive enough to generally account for ice particles with $D \geq 0.3$ mm, while ice particles with $D < 0.2$ mm were generally not measured.

Ice particles were classified according to the scheme suggested by Magono and Lee (1966). Due to mag-

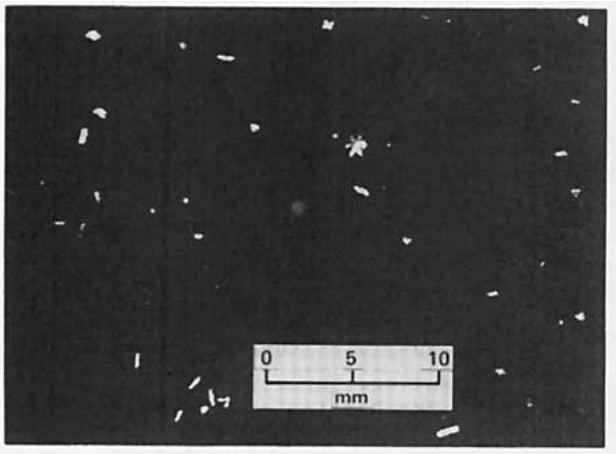

FIG. 1. Ice particles observed during the 1985–86 field season, showing long columns as the most abundant particle type.

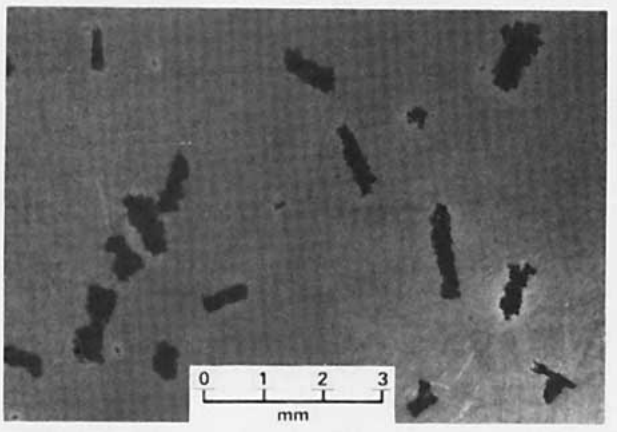

FIG. 3. Primarily rimed long columns from the 1986–87 field season, showing a diversity of aspect ratios.

nification differences, uncertainties in classifying ice particles in the 1985–86 dataset are generally greater than those in the 1986–87 dataset. The Magono and Lee scheme was amended somewhat to better accommodate information on riming and aggregation. Rimed ice particles in our scheme generally exhibited a greater degree of riming than a densely rimed plate in the Magono and Lee scheme, and we characterize the observed degrees of riming for our rimed particles as ranging from moderate to heavy. Examples of rimed and unrimed long columns sampled in this study are shown in Fig. 2. Aggregates were defined as ice particles consisting of two crystals or more. For each classified ice particle, we assigned a confidence factor of 1 to 4, a value of 1 indicating maximum confidence in ice particle type.

The mass of a snow particle was determined from the diameter of the drop (multiple drops in the case of an aggregate) into which it melted. Unambiguous identification of melt drops with the parent crystals was made by superimposing the ice particle images onto the drop images. Mass calculations assume that the drop is hemispherical in shape. To test this assumption, ice particles of various sizes, representative of those observed in the field, were melted on a plastic petri dish and photographed in the horizontal to expose their vertical dimensions. Examples of these melted ice particles are shown in Fig. 4, where it is seen that the droplets are hemispherical in shape.

In the cases in which sufficient data were available on a particular type of particle, a power law relation between the mass, m, and maximum dimension, D, of an ice particle was assumed:

$$m = \alpha D^{\beta}. \tag{1}$$

The terms α and β were determined by a least-squares fit to logarithms of mass and dimension:

$$\log m = \log\alpha + \beta \log D. \tag{2}$$

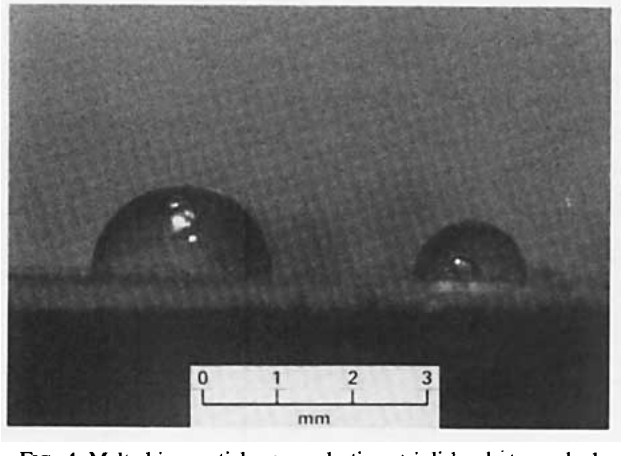

FIG. 4. Melted ice particles on a plastic petri dish, photographed in the horizontal to reveal their hemispherical shape.

Only ice particles classified with confidence values of 1 or 2 were used in developing these formulae.

3. Results

Empirical relationships based on our measurements between the mass and maximum dimension of various types of precipitation particles are listed in Table 1 for the 1986–87 field season and in Table 2 for the 1985–86 season. These expressions are valid only for the indicated size ranges. The exponent value for most ice particles was close to 2.0, as suggested in Table 1 by the expression for all ice particle types evaluated in the 1986–87 data. In both tables, we use the Magono and Lee classification C2b to represent aggregates of short columns, and not columnar bicrystals. In order to illustrate some of the natural scatter typically found in the data, mass-dimensional plots for short columns (C1e) and radiating assemblages of plates (P7a) are presented in Figs. 5 and 6 for the 1985–86 and the 1986–87 datasets, respectively. Individual data points are indicated.

From the correlation coefficients and the number of measurements, the probability that these relationships were not due to chance was >99.9%. Scatter in the data, however, yield rather high uncertainties for α and β. The uncertainty associated with α and β was examined by comparing the coefficients in Table 1 with those in Table 2 for the same particle types. The mean percentage difference between corresponding α coefficients was 31%, while the maximum difference was 75%. Similarly, the mean percentage difference between corresponding β values was 10%, while the maximum difference was 32%. Factors that would account for some of this variability including varying degrees of riming, differing aspect ratios and differing size ranges between the two populations of ice particles of a given classification. The different magnifications used in the two datasets may have also contributed to some of this variability, with greater uncertainty associated with data obtained at the lower magnification.

Cold-habit and warm-habit columns were differentiated by assuming conditions were near or above water saturation and by noting that, for these conditions, long columns are formed between −6 and −9°C (Pruppacher and Klett 1978, pp. 30–32). Also, short columns were often found associated with other cold habit crystals (i.e. bullets, capped columns, side planes). Thus, long columns (N1e) were classified as warm habit crystals and short columns (C1e) were classified as cold habit crystals.

Short columns were defined as having aspect ratios less than 2.0. A normalized frequency distribution of aspect ratios for long columns in the 1986–87 dataset is shown in Fig. 7. The mean value is 4.6. Figure 3, primarily featuring rimed, long columns, illustrates the diversity of aspect ratios typically encountered.

Ice particles not indicated as rimed in the 1986–87

TABLE 1. Mass-dimensional relationships for ice particles from the 1986–87 field season. Code is from Magono and Lee (1966).

Code	Particle type	Mass-size relationship[a]	Size range (mm)
N1a	Elementary needles*	$m = 0.0049L^{1.8}$ $N = 16, r = 0.84$	0.6 to 2.7
R1a	Rimed elementary needles*	$m = 0.0060L^{2.1}$ $N = 7, r = 0.9723$	0.5 to 2.8
N1e	Long columns*	$m = 0.012L^{1.8}$ $N = 64, r = 0.71$	0.2 to 1.5
R1b	Rimed long columns	$m = 0.023L^{1.8}$ $N = 27, r = 0.83$	0.2 to 2.4
N2c	Combinations of long columns*	$m = 0.017L^{1.8}$ $N = 62, r = 0.87$	0.2 to 2.6
	Rimed combinations of long columns*	$m = 0.025L^{1.9}$ $N = 54, r = 0.90$	0.3 to 4.9
C1e	Short columns*	$m = 0.064L^{2.6}$ $N = 12, r = 0.92$	0.2 to 0.6
C2b	Combinations of short columns*	$m = 0.031L^{1.9}$ $N = 17, r = 0.86$	0.4 to 1.4
P1a	Hexagonal plates*	$m = 0.028D^{2.5}$ $N = 30, r = 0.88$	0.2 to 1.0
P7a	Radiating assemblages of plates*	$m = 0.019D^{2.1}$ $N = 63, r = 0.92$	0.2 to 3.0
S1	Side planes	$m = 0.021D^{2.3}$ $N = 77, r = 0.95$	0.3 to 2.5
R3b	Heavily rimed dendritic crystals	$m = 0.068D^{2.2}$ $N = 20, r = 0.95$	0.2 to 2.8
	Fragments of heavily rimed dendritic crystals*	$m = 0.027D^{1.7}$ $N = 39, r = 0.83$	0.3 to 1.9
	Aggregates of side planes	$m = 0.021D^{2.2}$ $N = 35, r = 0.93$	0.6 to 4.1
S3	Aggregates of side planes, bullets and columns	$m = 0.022D^{2.1}$ $N = 31, r = 0.94$	0.8 to 4.5
	Aggregates of radiating assemblages of plates*	$m = 0.023D^{1.8}$ $N = 30, r = 0.91$	0.8 to 7.7
	Aggregates of fragments of heavily rimed dendritic crystals*	$m = 0.034D^{2.0}$ $N = 46, r = 0.89$	0.5 to 4.8
	All above snow types	$m = 0.022D^{2.0}$ $N = 643, r = 0.89$	0.2 to 7.7

[a] Mass m is given in milligrams and maximum dimension D or L is given in millimeters; N is the number of data points; r is the correlation coefficient for the relationship.

* No previously reported relationship.

dataset may be either unrimed or lightly rimed particles, since ice particles exhibiting light degrees of riming were still classified as unrimed. For the 1985–86 dataset, only heavy riming was probably detectable in most cases, due to the lower magnification used.

4. Discussion

a. *Relationship between ice crystal aspect ratio and the exponent β*

If each crystal of a given habit grew in a cloud such that its a- and c-axes were always proportional to each other, then β should equal 3.0 for that crystal habit. For example, if the aspect ratio is $k = c/a$, the volume of a hexagonal prism can be given approximately as

$$V = \pi r^2 kr, \tag{3}$$

where r is the radius of a circle having an area equivalent to the basal face and kr is the length of the column. If k is constant for all sizes of this habit, then the crystal mass, m, should be proportional to r^3 for this classification, provided ice densities do not change much with size. The fact that ice crystal growth rates usually cause crystal axes to evolve disproportionally makes k variable and accounts for $\beta \leqslant 3$ (see Tables 1 and 2). Hence, the more the ice crystals of a given habit tend to grow at a constant aspect ratio, the greater the value of β will be. This presumes that changes in ice density are not too severe. The higher exponents associated with short columns and hexagonal plates in Table 1 might reflect growth rates along crystal axes that promote more constant aspect ratios.

b. *Effect of riming and aggregation*

As one might expect, riming was found to increase the mass of an ice particle of given size and type. The rimed ice particles examined in this study were gen-

TABLE 2. Mass-dimensional relationships for ice particles from the 1985–86 field season.

Code	Particle type	Mass-size relationship[a]	Size range (mm)
N2c	Combination of long columns*	$m = 0.026L^{1.9}$ $N = 124, r = 0.67$	0.3 to 2.1
C1e	Short columns*	$m = 0.045L^{2.1}$ $N = 59, r = 0.77$	0.2 to 1.0
C2b	Combinations of short columns*	$m = 0.033L^{1.8}$ $N = 168, r = 0.66$	0.3 to 1.7
CP1a	Capped columns*	$m = 0.046L^{1.9}$ $N = 16, r = 0.75$	0.4 to 1.0
P1a	Hexagonal plates*	$m = 0.043D^{1.8}$ $N = 35, r = 0.63$	0.3 to 1.2
R3b	Heavily rimed dendritic crystals	$m = 0.031D^{1.9}$ $N = 75, r = 0.86$	0.5 to 3.7
	Fragments of heavily rimed dendritic crystals*	$m = 0.028D^{1.8}$ $N = 205, r = 0.76$	0.4 to 3.5
	Aggregates of fragments of heavily rimed dendritic crystals*	$m = 0.028D^{1.9}$ $N = 49, r = 0.82$	0.7 to 6.2
	All above snow types	$m = 0.030D^{1.7}$ $N = 795, r = 0.81$	0.2 to 6.2

[a] Mass m is given in milligrams and maximum dimension D or L is given in millimeters; N is the number of data points; r is the correlation coefficient for the relationship.

* No previously reported relationship.

erally moderately to heavily rimed, as shown in Figs. 2 and 3. Riming had the effect of increasing the value of α. Riming appeared to have no significant effect on the value of β, although this is based only on columnar ice particles.

Aggregation appears to affect ice particle mass-dimensional relations by changing the particle shape and the bulk density. Bulk densities are defined here as the ice particle mass divided by the volume of a sphere described by its maximum dimension. In Fig. 8, best fit lines are presented from Table 1 data which describe mass-size relations for aggregates of long and short columns and their component crystals. For a given particle size, aggregates have less mass for short columns, but more mass for long columns. This suggests that, for low aspect ratio crystals such as short columns, aggregation tends to decrease bulk densities. Conversely, for high aspect ratio crystals such as long columns, aggregation may effectively increase the shorter dimension, thus increasing bulk densities. For long columns, aggregation increased masses up to 40%, while for short columns, aggregation decreased masses up to 40%. For

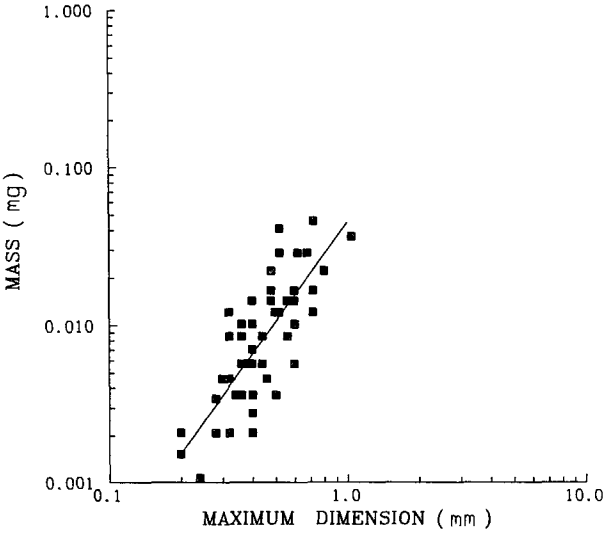

FIG. 5. Mass-size plot for short columns (C1e), using the 1985–86 dataset, showing the least-squares fit line.

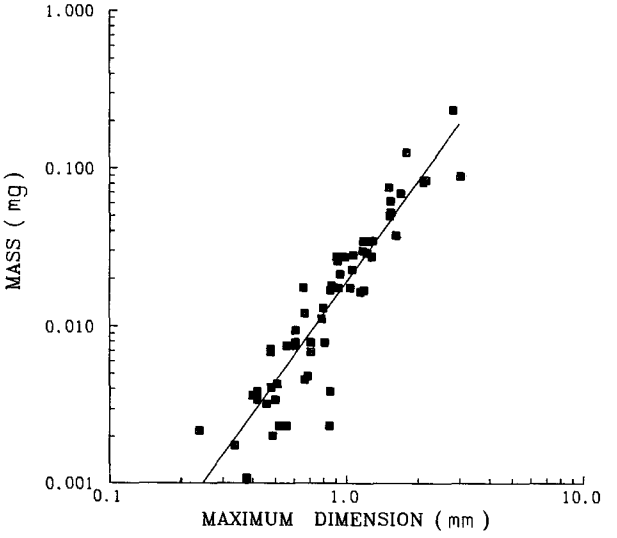

FIG. 6. Mass-size plot for radiating assemblages of plates (P7a), using the 1986–87 dataset, showing the least-squares fit line.

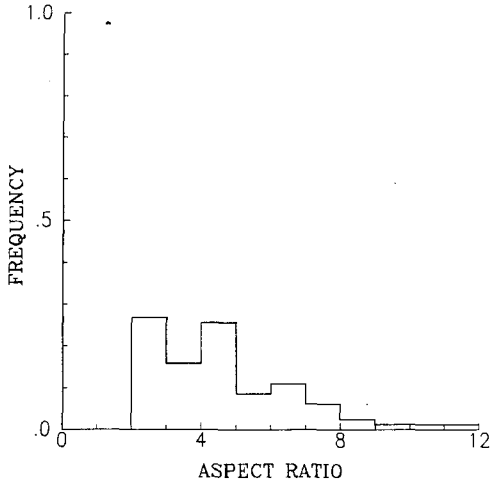

FIG. 7. Normalized frequency distribution of aspect ratios for long columns in the 1986–87 dataset.

aggregated planar crystals, aggregation appeared to have no significant functional effect on their masses. Hence, based on these data, the effect of aggregation on mass for a given snow type and size appears to be minor. With the exception of short columns (C1e) in the 1986–87 data, aggregation had only a minor effect, if any, on α and β. However, aggregates examined during this study were generally not composed of many crystals.

c. *Comparisons with other studies*

Mass-dimensional expressions for individual ice crystals have also been derived from the data provided by others, specifically Heymsfield (1972) and Auer and Veal (1970). These relationships, obtained from geometric and density data, are compared with those from this study. Our results are then compared with mass-dimensional relations reported by Locatelli and Hobbs (1974).

1) EXPRESSIONS FOR INDIVIDUAL CRYSTALS

By assuming the simple geometry of a cylindrical shape for the crystal, one can formulate the crystal mass in terms of its volume and density:

$$m = (\pi/4)D^2 L\rho_i \qquad (4)$$

where D is the crystal width for columnar crystals and diameter for planar crystals, L the length or thickness of the ice particle, and ρ_i the crystal density. Using the ice crystal dimensional relations given by Auer and Veal (1970) and Heymsfield (1972), and the density relations of Heymsfield (1972), Eq. (4) can be used to approximate mass-dimensional relationships for single crystals. The results are shown in Table 3. Unfortunately, such an approach for calculating the crystal mass can be used only for limited types of particles, and is not sufficiently accurate to estimate the masses of aggregates or heavily rimed crystals. However, it does provide a point of comparison for some of the expressions in this study.

Figure 9 contains our best fit lines for needles and columnar crystals, taken from Table 1, together with lines derived from Eq. (4). It is seen that the slopes for all crystal habit pairs agree fairly well. Crystal masses differ by a factor of two or less between the empirical and derived expressions, for a given habit and size. This may be due to differences in aspect ratios, with lower aspect ratios exhibiting greater masses for a given size. This may also explain the 50% increase in mass for combinations of long columns in Table 2 relative to Table 1. Figure 9 shows that there is a tendency for the lines plotted for columns (C1e, N1e) to converge at a crystal size near 0.2 mm. This may reflect the tendency of columnar crystals to exhibit similar aspect ratios at these smaller sizes.

The expression for plates (P1a) in Table 1 agrees extremely well with the derived expression for hexagonal plates. In view of this and the fact that the correlation coefficient for plates in Table 2 was the lowest for this study suggests that the expression for plates given in Table 1 is the more reliable.

2) COMPARISON OF RIMED PARTICLES

Shown in Fig. 10 are mass-size relations for heavily rimed dendritic crystals (i.e. graupel-like snow of lump type) and rimed columns from the present study (Table 1) and from Locatelli and Hobbs (1974). Strong agreement was found between this study and that of Locatelli and Hobbs for heavily rimed dendritic crystals. The agreement regarding rimed columns appears

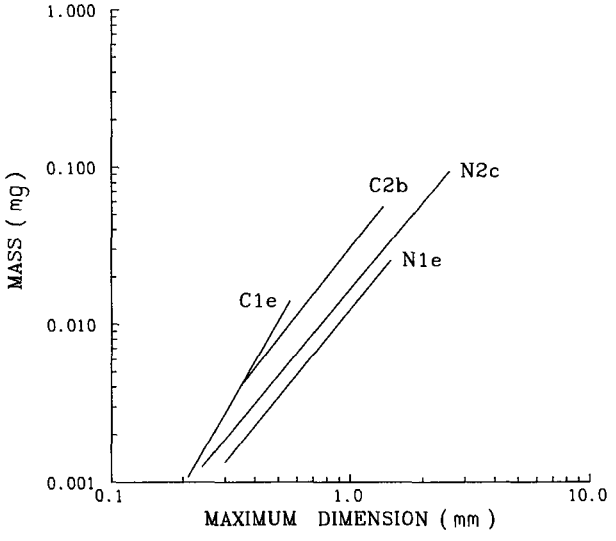

FIG. 8. Best fit lines from our Table 1 data for short columns (C1e), short column aggregates (C2b), long columns (N1e) and long column aggregates (N2c). Observed size ranges are indicated.

TABLE 3. Dimensional relations, densities and derived mass-size relations for different crystal forms. Maximum dimensions are used, where L = length for columns and needles.

Crystal type	Width (mm)	Density (g cm^{-3})	Mass-size relation (size: mm, mass: mg)
Column			
Cold Region (C1e)	*$0.5L$, $L < 0.3$	*$0.65L^{-0.0915}$	$m = 0.13L^{2.9}$
(N1e)	*$0.197L^{0.414}$, $L > 0.2$	*$0.65L^{-0.0915}$	$m = 0.025L^{1.7}$
Warm Region (N1e)	*$0.197L^{0.414}$, $L > 0.2$	*$0.85L^{-0.014}$	$m = 0.026L^{1.8}$
Hexagonal Plate (P1a)	†$0.0449D^{0.449}$	*0.9	$m = 0.032D^{2.5}$
Needle (N1a)	†$0.0747L^{0.611}$	*$0.6L^{-0.117}$	$m = 0.001L^{2.1}$

* Results from Heymsfield (1972).
† Results from Auer and Veal (1970).

fairly good, with the small mass differences possibly resulting from differences in aspect ratios. The rimed columns in this study were characterized by aspect ratios generally between 2 and 7, while aspect ratios in the Locatelli and Hobbs study were not mentioned. A lower aspect ratio should yield greater mass for a given maximum dimension. The higher correlation coefficient for short columns (C1e) than for long columns (N1e) in Table 1 may partially reflect the narrower range of aspect ratios (between 1 and 2) for short columns.

3) COMPARISON OF AGGREGATES

Plotted in Fig. 11 are the best-fit curves for two types of aggregates from the present study and that of Locatelli and Hobbs. This study shows that the masses of aggregates of side planes fall on almost the same line as those of aggregates that include side planes, bullets and columns. Although the slopes from the two studies differ regarding side plane aggregates, the masses predicted by the two lines agree within a factor of 2.5 or better. The two lines describing aggregates of side planes, bullets and columns agree fairly well, with predicted masses for aggregates of a given size agreeing within a factor of 2 or better (within the size range common to both studies).

Another study by You et al. (1987) reported mass-dimensional relationships for side planes, bullet rosettes, spatial dendrites, and planar dendritic crystals (the latter comprising 15 Magono and Lee classifications). Only the side plane category is common to this study. Unfortunately, S1 and S3 particle types were combined to represent side planes in their study, and no information on riming or aggregation was given in their classification scheme. Nonetheless, their coefficients for side planes compare favorably with ours, with $\alpha = 0.022$ and $\beta = 1.8$.

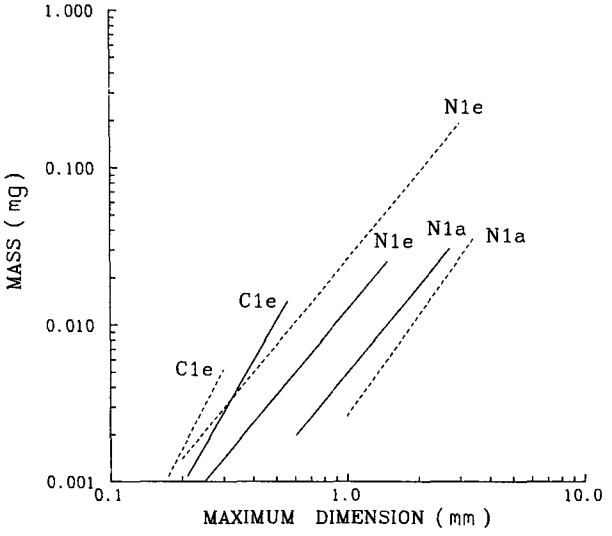

FIG. 9. Best fit lines from our Table 1 data (solid lines) and lines from the derived expressions in Table 3 (dashed lines) for their corresponding size ranges. Crystal habits plotted are short columns (C1e), long columns (N1e) and needles (N1a).

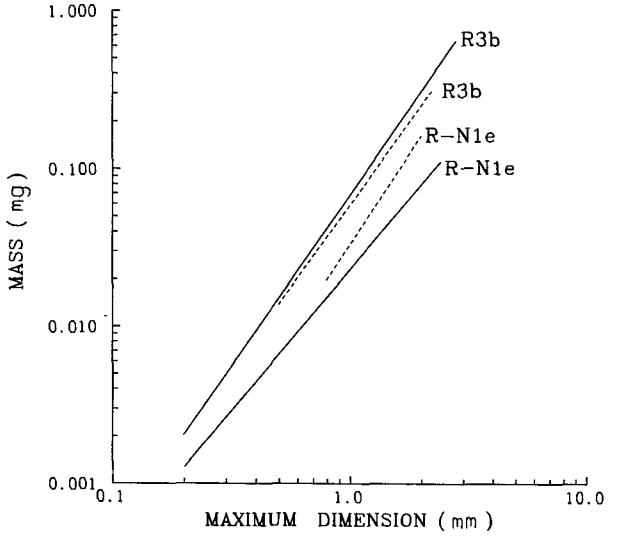

FIG. 10. Best fit lines from our Table 1 data (solid lines) and from the data of Locatelli and Hobbs (dashed lines). Snow types plotted are heavily rimed dendritic crystals (R3b) and rimed columns (R-N1e). Columns were not characterized by aspect ratios in the Locatelli and Hobbs study.

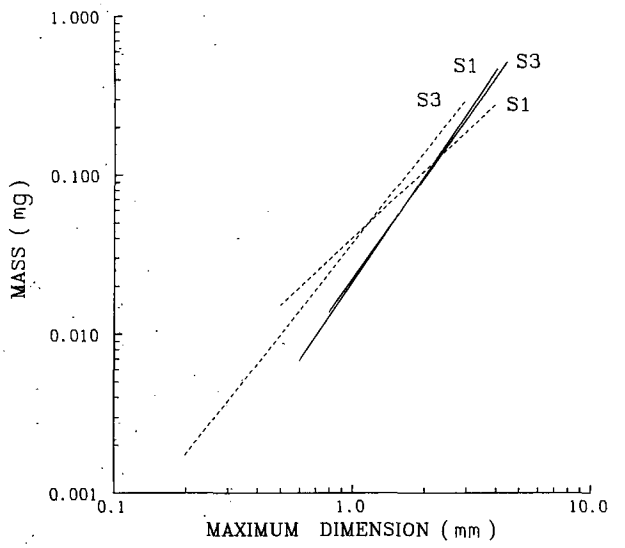

FIG. 11. Best fit lines from our Table 1 data (solid lines) and from the data of Locatelli and Hobbs (dashed lines) for aggregate snow. Lines labeled S1 refer to aggregates of side planes, while lines labeled S3 refer to aggregates of side planes, bullets and columns.

d. The contribution of cloud droplet accretion to the snowfall rate

In this section, an expression is derived to estimate the mass fraction of the snowpack due to rimed cloud droplets. The expression uses some of the mass-dimensional relations for rimed and unrimed particles developed here. In the derivation, the mass fraction of the snowpack composed of accreted cloud water is taken to be identical to the fraction of the mass flux of snowfall due to riming. The derivation also treats the snowfall as being comprised of a single ice crystal habit type (i.e. rimed and unrimed long columns), since there are few particle types in our dataset for which both rimed and unrimed mass-dimensional expressions are available. Restricting the derivation to a particular snow type avoids complications associated with ice particle shape when estimating the contribution of riming to the snowfall rate. Although other particle types not used here could influence the results, shape effects appear to be of second order in importance relative to liquid water contents and cloud droplet size distributions in determining the mass fraction of the snowpack due to riming (Pruppacher and Klett 1978, pp. 495–500). The study of Feng et al. (1982) has the same limitation, and it is hoped that future investigators can address some of the particle types we have not.

The mass fraction of the snowpack due to accreted cloud water, f_{cw}, may be expressed as

$$f_{cw} = F_{cw}/F_t \tag{5}$$

where F_{cw} is the mass flux of accreted cloud water and F_t is the total ice particle mass flux. The flux of accreted cloud water may be estimated by subtracting from the rimed ice particle mass flux the component of this mass flux due to diffusional growth. In terms of ice mass contents, this is the same as subtracting the diffusional ice mass component from the ice mass concentration consisting of rimed ice particles, and multiplying this difference by the rimed-particle mean fallspeed:

$$F_{cw} = v_r(X_r - X'_r) \tag{6}$$

where X_r is the rimed ice particle mass concentration in the falling snow, X'_r is an estimate of the diffusional part of the rimed ice particle mass concentration, and v_r is the mass mean fallspeed for rimed ice particles. The total ice particle mass flux may be divided into its rimed and unrimed ice particle components,

$$F_t = F_r + F_u. \tag{7}$$

These components may also be expressed in terms of their mass concentrations:

$$F_r = v_r X_r, \tag{8}$$

$$F_u = v_u X_u, \tag{9}$$

where X_u is the mass concentration for unrimed ice particles and v_u is the mass mean fallspeed for unrimed ice particles.

Using Eqs. (5) through (9), the fraction of the snowpack mass due to accreted cloud water may be expressed as

$$f_{cw} = \frac{v_r(X_r - X'_r)}{v_u X_u + v_r X_r}. \tag{10}$$

An applied form of Eq. (10) can be derived using mass-dimensional relationships from this study, since the ice mass content, χ, of a given snowfall event can be expressed as

$$\chi = \int_{D_{\min}}^{D_{\max}} m(D)n(D)dD$$

$$= \int_{D_{\min}}^{D_{\max}} \alpha D^{\beta} n(D)dD \tag{11}$$

where $n(D)dD$ is the concentration of ice particles with diameters between D and $D + dD$, and $D_{\min}$ and $D_{\max}$ are the smallest and largest ice particle sizes. The rimed ice particle mass concentration, X_r, and its diffusional component, X'_r, may be expressed as

$$X_r = \int_{D_{\min}}^{D_{\max}} \alpha_r D^{\beta_r} f_r n(D)dD, \tag{12}$$

$$X'_r = \int_{D_{\min}}^{D_{\max}} \alpha_u D^{\beta_u} f_r n(D)dD \tag{13}$$

where the subscripts r and u refer to rimed and unrimed snow, respectively, and where f_r is the number fraction of rimed ice particles in a given size interval. Since $n(D)$ is for all ice particles, the product $f_r n(D)dD$ represents the number of rimed ice particles within a given

size interval. When this product is multiplied by the rimed mass expression, the mass concentration of rimed particles within a size interval is obtained, and when multiplied by the unrimed mass expression, the diffusional mass component of rimed ice particles within a size interval is obtained. If f_r is not a function of ice particle size, then for snow containing both rimed and unrimed ice particles of a given type, the downward flux of accreted cloud water may be estimated as

$$F_{cw} = f_r v_r (\chi_r - \chi_u), \tag{14}$$

where

$$\chi_r = \int_{D_{min}}^{D_{max}} \alpha_r D^{\beta_r} n(D) dD, \tag{15}$$

$$\chi_u = \int_{D_{min}}^{D_{max}} \alpha_u D^{\beta_u} n(D) dD, \tag{16}$$

and where f_r is the ratio of the concentration of rimed ice particles to all ice particles. Note that χ_r is defined such that all ice particles are rimed, while χ_u is defined such that all ice particles are unrimed.

The use of f_r in (14) assumes that the probability of finding rimed ice particles in a given size interval is the same as for unrimed particles. This assumption is supported by the present data, as seen in Fig. 12, which shows normalized size-frequency plots for the rimed and unrimed ice particles contained in the 1986–87 dataset. The frequency distributions for the rimed and unrimed ice particles show no obvious differences. Furthermore, from Figs. 13 and 14, the general increase in ice particle mass due to riming does not appear sensitive to ice particle size over the sizes reported here (note the identical or similar slopes, or their corresponding β values in Table 1). For columns with $D > 0.2$ mm, and for plates with $D > 0.5$ mm, numerical

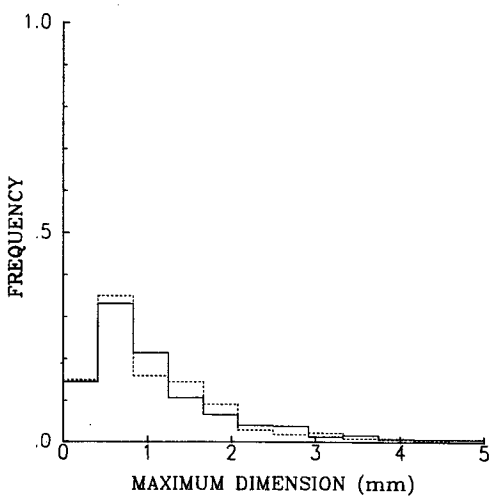

FIG. 12. Normalized frequency-size distributions for all unrimed (solid line) and rimed (dashed line) ice particles in the 1986–87 dataset. For unrimed particles $N = 571$. For rimed particles $N = 294$.

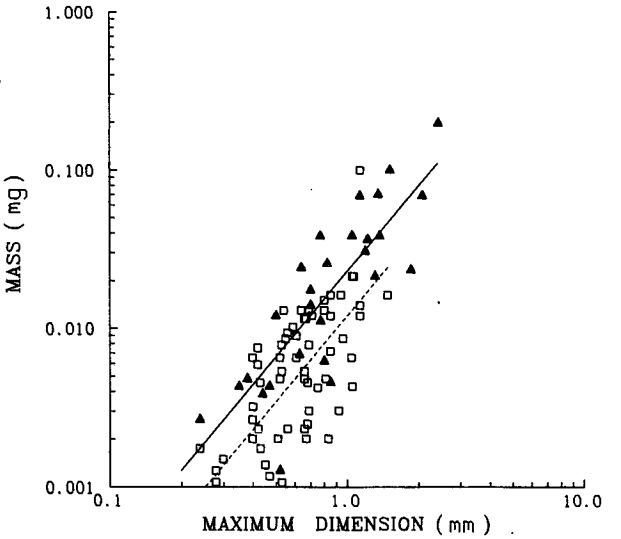

FIG. 13. The influence of riming on the mass of single ice crystals. Plotted are the masses of long columns (squares, dashed line) and rimed long columns (triangles, solid line).

work (Pruppacher and Klett 1978, pp. 495–499) indicates that collision efficiencies do not vary much between cloud droplets > 20 μm of a given size and the crystals. Experimental work on ice crystals and aggregates (Lew et al. 1986; Kajikawa 1974; Murakami 1985) indicates that collision efficiencies can still be appreciable at droplet sizes as small as 5 μm (up to ~0.2), increasing with decreasing crystal sizes. Riming of small crystals (>0.2 mm) by smaller droplets could then be significant in view of the higher concentrations of the smaller droplets. To estimate f_r for a given snowfall event, the number of rimed particles analyzed for

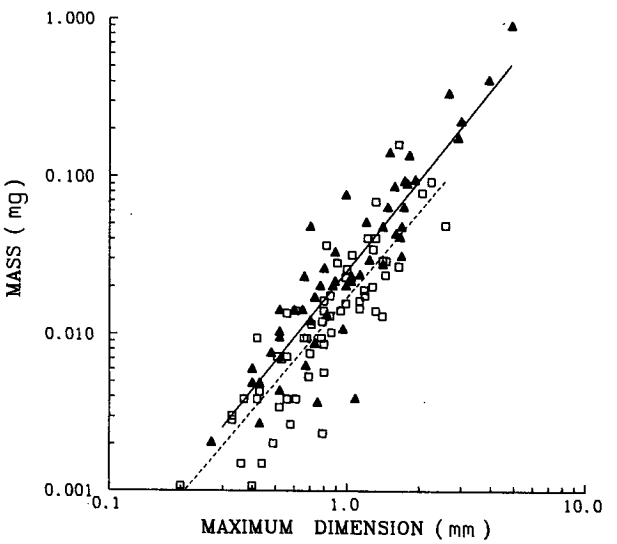

FIG. 14. The influence of riming on the mass of aggregates. Plotted are the masses of long column aggregates (squares, dashed line) and rimed long column aggregates (triangles, solid line).

that event was divided by the total number of ice particles.

The flux terms F_r and F_u may be treated analogously to F_{cw}. Since X_r may be represented as $f_r\chi_r$ and X_u as $(1-f_r)\chi_u$, then

$$F_r = f_r v_r \chi_r \tag{17}$$

and

$$F_u = (1-f_r) v_u \chi_u \tag{18}$$

where $n(D)$ in χ_r and χ_u is the same. Substituting into Eq. (5), Eqs. (14), (17), and (18) can be combined to give

$$f_{cw} = \frac{K f_r(\chi_r - \chi_u)}{(1-f_r)\chi_u + K f_r \chi_r} \tag{19}$$

where v_r has been expressed as Kv_u. Zikmunda and Vali (1972) have estimated that $K \approx 2$, while Locatelli and Hobbs (1974) indicate K may be *as high as* 2 (i.e. for heavy riming). For the moderate to heavily rimed snowfall observed during this study, it was assumed that $K = 1.5$. Note that when most ice particles are rimed during an event ($f_r \Rightarrow 1.0$), the terms f_r and K drop out of (19), and $f_{cw} \Rightarrow 1 - \chi_u/\chi_r$.

The relationships for rimed and unrimed long columns, and for rimed and unrimed combinations of long columns (found in Table 1) may be used to evaluate (19). These relationships (plotted in Figs. 13 and 14) indicate that rimed particles generally possess greater masses for the same particle type and size. The expressions for rimed and unrimed needles were not used due to the sparsity of data on rimed needles.

In calculating χ_r and χ_u, the frequency distributions in Fig. 12 were converted to size distributions by multiplying each bin value by 0.1 cm^{-4} to yield reasonable concentrations. The average of the resulting distributions was used to represent $n(D)$. Since the smallest particles (i.e. $D < 0.2$ mm) are generally not counted by our measurement technique, the distributions in Fig. 12 could be more exponential than they appear. However, the use of the same size distribution in the numerator and denominator of (19) results in f_{cw} being unaffected by the choice of size distribution. This was demonstrated by using an exponential size distribution with a differing χ to evaluate (19), where it was found that f_{cw} was unchanged.

The integrals in (15) and (16) were numerically evaluated over the size range common to both rimed and unrimed long columns (see Table 1). Neglecting ice particles with $D < 0.2$ mm should not effect results much. If the first bin in Fig. 12 (i.e. smallest particles) was 0.60 instead of 0.15, particles < 0.2 mm would contribute <1% of the total mass in the distribution. After integration, it was found that $\chi_r = 0.0471$ g m^{-3} and that $\chi_u = 0.0246$ g m^{-3}. For the case study of 18 December 1986, characterized by moderate to heavily rimed snowfall, f_r was found to be 0.73, giving $f_{cw} = 0.42$ for long columns. When long column combinations were used, $\chi_r = 0.133$ g m^{-3}, $\chi_u = 0.0744$ g m^{-3} and $f_{cw} = 0.30$. Averaging the above two values of f_{cw}, it appears that accreted cloud water contributed about 36% of the mass to the fresh snowpack.

For another moderately rimed snowfall event on 22 December 1986, f_r was found to be 0.58. Repeating the above analysis, the mean estimate for f_{cw} was 0.32.

Considerable uncertainty is associated with the value assigned to K. However, an uncertainty of ±0.5 in K (±33%) results in an uncertainty of ±2% in f_{cw} for the 18 December event and ±3% for the 22 December event.

1) Comparisons with other studies

The estimates from this study are somewhat lower than the estimates of Feng and Grant (1982), Harimaya and Sato (1989), and Marwitz (1986), which suggest that accreted cloud water represents about one half or more of the mass flux during rimed snowfall. Such differences are not surprising, however, considering the differing methods used and the variability in the degree of ice particle riming between and within storms. The importance of riming during a storm should depend on the time during which riming occurred. The two storms examined here were characterized by shallow orographic clouds, with cloud depths of 1.5 to 3 km. If the layer in which riming occurred was shallower in these clouds than in the clouds corresponding to the above mentioned studies, this may explain in part the slightly different results. Of course, the liquid water content and droplet distribution are also important factors that are missing from this and the other field studies. Estimates of the riming contribution in this study may be conservative since some of the particles used in our "unrimed" category were lightly rimed (i.e. exhibiting less riming than a densely rimed crystal in the Magono and Lee scheme).

The study by Harimaya and Sato (1989) was similar to this one in that it was based on mass-dimensional relationships for three different ice crystal riming categories. However, these relationships were not based on a single crystal type as in this study, but rather were based on the degrees of riming for all observed crystals. They estimated that riming contributed about 40 to 60% of the ice mass for rimed snowflakes. But when graupel particles were considered in addition to snowflakes, it was estimated that accreted cloud water generally represents 60 to 95% of the snow mass sampled in this coastal region of Japan.

2) Related issues

From the above mentioned studies and this one, it appears that a large fraction of the mass in snowfall may be accreted cloud water. It is generally recognized

that anthropogenic emissions have the potential to enhance cloud condensation nuclei concentrations, increase cloud droplet concentrations and decrease mean cloud droplet sizes (Borys et al. 1988; Coakley et al. 1987; Hudson 1980). Since small cloud droplets are less likely to impact on ice particles than larger droplets, the efficiency of the riming process and the precipitation process overall could be significantly diminished by the modification of droplet size distributions through anthropogenic emissions.

5. Summary

Observations of the maximum dimensions and masses of ice particles, collected during snowfall in the Sierra Nevada, have provided a variety of new mass-dimensional relationships for ice particles. These relationships were compared, where possible, with other mass-dimensional expressions in the literature for the same ice particle type. These comparisons indicate that the results of this study are in general agreement with the existing body of information on mass-dimensional relationships.

Mass-dimensional relationships for rimed and unrimed columns and column aggregates were incorporated into an expression for the ice mass concentration. These ice mass content expressions for rimed and unrimed snow were then combined to yield an equation which estimates the mass fraction of the fresh snowpack comprised of accreted cloud droplets. For the two snowfall events examined here, it was estimated that accreted cloud water constituted 30 to 40 percent of the mass of the fresh snow. Additional mass-dimensional relationships for rimed and unrimed ice particles of the same type would be useful in making similar assessments.

Acknowledgment. Part of the field work was supported by the Department of Interior's Bureau of Reclamation under Cooperative Agreement 5-FC-81-05880. The remaining field program and analysis effort were supported by NOAA under contract NA88-RAH08126. Both institutes are thanked for their support. The authors would like to thank Dr. Dennis Lamb, Dr. Joseph Warburton, Dr. Randolph Borys, Dr. Steven Chai and some anonymous reviewers for their helpful comments.

REFERENCES

Auer, A., and D. Veal, 1970: The dimensions of ice crystals in natural clouds. *J. Atmos. Sci.*, **27**, 919–926.

Bashkirova, G. M., and T. A. Pershina, 1964: On the mass of snow crystals and their fall velocity. *Tr. Gl. Geofiz. Observ.*, Engl. Transl., No. 165, 83–100.

Borys, R. D., E. E. Hindman and P. J. DeMott, 1988: The chemical fractionation of atmospheric aerosol as a result of snow crystal formation and growth. *J. Atmos. Chem.*, **7**, 213–239.

Coakley, J. A., Jr., R. L. Bernstein and P. A. Durkee, 1987: Effect of ship stack effluents on cloud reflectivity. *Science*, **237**, 1020–1022.

Feng, D., and L. O. Grant, 1982: Correlation of snow crystal habit, number flux and snowfall intensity from ground observations. Preprints, Conf. on Cloud Physics, Amer. Meteor. Soc., Boston, Massachusetts, 485–487.

Harimaya, T., and M. Sato, 1989: Measurement of the riming amount on snowflakes. *J. Fac. Sci., Hokkaido Univ., Ser. VII*, **8**, 355–366.

Herzegh, P. H., and P. V. Hobbs, 1981: The mesoscale and microscale structure and organization of clouds and precipitation in mid-latitude cyclones. IV: Vertical air motions and microphysical structure of prefrontal surge clouds and cold-frontal clouds. *J. Atmos. Sci.*, **38**, 1771–1784.

Heymsfield, A., 1972: Ice crystal terminal velocities. *J. Atmos. Sci.*, **29**, 1348–1357.

Hudson, J. G., 1980: Relationship between fog condensation nuclei and fog microstructure. *J. Atmos. Sci.*, **37**, 1854–1867.

Kajikawa, M., 1974: On the collection efficiency of snow crystals for cloud droplets. *J. Meteor. Soc. Japan*, **52**, 328–335.

Leighton, H. G., 1980: A comparison of a numerical model and an approximate analytical model of the growth of snowflakes. *J. Atmos. Sci.*, **37**, 1409–1411.

Lew, J. K., D. C. Montague and H. R. Pruppacher, 1986: A wind tunnel investigation on the riming of snowflakes. Part II: Natural and synthetic aggregates. *J. Atmos. Sci.*, **43**, 2392–2409.

Locatelli, J. D., and P. V. Hobbs, 1974: Fallspeeds and masses of solid precipitation particles. *J. Geophys. Res.*, **79**, 2185–2197.

Magono, C., and C. V. Lee, 1966: Meteorological classification of natural snow crystals. *J. Fac. Sci. Hokkaido Univ., Ser. 7*, no. 2, 321–362.

Marwitz, J. D., 1986: Deep orographic storms over the Sierra Nevada. Part II: The precipitation processes. *J. Atmos. Sci.*, **44**, 174–185.

Mitchell, D. L., 1988: Evolution of snow-size spectra in cyclonic storms. I: Snow growth by vapor deposition and aggregation. *J. Atmos. Sci.*, **45**, 3431–3451.

Murakami, M., 1985: Experiments on aerosol scavanging by natural snow crystals. Part I: Collection efficiency of uncharged snow crystals for micron and submicron particles. *J. Meteor. Soc. Japan*, **63**, 119–128.

Nakaya, U., and T. Terada, 1935: Simultaneous observation of the mass, falling velocity and form of snow crystals. *J. Fac. Sci. Hokkaido Univ., Ser. 2*, no. 1, 191–201.

You, L., Y. Chen and T. Wang, 1987: A study on the relationship between the masses and dimensions of snow crystals. *J. Academy Meteor. Sci.*, **2**, 197–201 (in Chinese).

Zikmunda, J., and B. Vali, 1972: Fall patterns and fall velocities of rimed ice crystals. *J. Atmos. Sci.*, **29**, 1334–1347.